Femtosecond Pulse Shaping for Synthesis, Processing, and Time-to-Space Conversion of Ultrafast Optical Waveforms

Andrew M. Weiner, *Fellow, IEEE,* and Ayman M. Kan'an

(Invited Paper)

***Abstract*— Shaping, signal processing, and time–space conversion of femtosecond pulses can be achieved by linear and nonlinear manipulation of the spatially dispersed optical frequency spectrum within a grating and lens pulse shaper. In this paper, we first review our work on femtosecond pulse shaping and processing, with an emphasis on applications to high-speed communications and information processing. We then present a new concept for generalized time–space processing based on cascaded time-to-space and space-to-time conversions in conjunction with smart pixel optoelectronic arrays and provide a detailed discussion of our recent studies of time-to-space conversion based on second-harmonic generation (SHG) within a femtosecond pulse shaper.**

***Index Terms*— Demultiplexing, holography, nonlinear optics, optical pulse measurements, optical pulse shaping, second harmonic generation, ultrafast optics.**

I. Introduction

REVOLUTIONARY breakthroughs have occurred in the field of ultrafast laser technology during the 1990's. Mode-locked dye lasers have given way to mode-locked solid-state lasers, which offer substantially increased average powers ($\sim$1 W and above), shorter pulsewidths (below 10 fs), as well as extremely high-peak powers in amplified systems. The use of solid-state gain media has also led for the first time to simple, turn-key femtosecond lasers, and many researchers are now setting their sights on practical and low-cost ultrafast laser systems suitable for real-world applications.

At the same time, important advances have also occurred in the complementary areas of ultrafast optical pulse-shaping, waveform synthesis, and signal processing, which are the subject of this paper. Using pulse-shaping techniques, one can now engineer femtosecond pulses into complex optical signals according to specification. A key point is that waveform synthesis is achieved by parallel modulation in the frequency domain, which is achieved by spatial modulation of the spatially dispersed optical frequency spectrum. Thus, waveforms with effective serial modulation bandwidths as high as terahertz can be generated without requiring any ultrafast modulators. Furthermore, by using an extension of pulse shaping called spectral holography, one can holographically record and then reconstruct such waveforms. During the reconstruction process, one can also perform interesting signal processing operations, such as time reversal, convolution, correlation, and matched filtering of femtosecond optical waveforms. Holographic methods also allow time-to-space conversion, where ultrafast time-domain signals are mapped (demultiplexed) into a spatial replica of the original ultrafast waveform.

These time/spectral-domain processing methods are in close analogy with traditional spatial-domain Fourier optics processing techniques. By applying such Fourier processing methods in the ultrafast time domain, one can achieve many new capabilities not available using other approaches.

One aim of our current research is to expand on this relationship between space and time to develop generalized time–space processing systems. The key concept is to first convert incoming ultrafast time-domain optical signals into spatial optical signals. In the spatial domain these signals can then be processed in parallel using optoelectronic smart pixel array technologies, and finally converted back into the ultrafast time domain. The use of smart pixel optoelectronics may allow sophisticated digital electronic processing operations which would not be possible directly in the ultrafast optical domain. This may have important applications, e.g., for processing of information in ultrahigh-speed optical communications networks.

In Section II of this paper, we review our work on femtosecond waveform synthesis and holographic processing of femtosecond optical waveforms, with an emphasis on applications to high-speed communications and information processing. A detailed review of work in this field up to $\sim$1995 is given in [1]. In Section III, we then outline our current research on generalized time—space processing systems. A key issue in applying such methods for real applications is the response time of the space-to-time and time-to-space converters, which should be able to operate at frame rates in the gigabit-per-second range. A time-to-space conversion technique that can meet this requirement was recently demonstrated in [2], [3], where the time-to-space conversion was accomplished by using a modified spectral holography approach where a second-harmonic crystal acts as the "holographic" (actually

Manuscript received October 24, 1997. This work was supported by the Air Force Office of Scientific Research under Contract F49620-95-1-0533 and by the National Science Foundation under Grant ECS-9312256.

The authors are with the School of Electrical and Computer Engineering, Purdue University, West Lafayette, IN 47907-1285 USA.

Publisher Item Identifier S 1077-260X(98)03781-2.

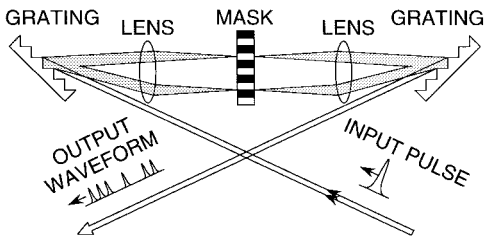

Fig. 1. Femtosecond pulse-shaping apparatus.

nonlinear) medium. We have adopted this approach in our laboratory and have investigated how to optimize the conversion efficiency of the second-harmonic generation (SHG) based time-to-space converter [4]. We have recently achieved greater than 50% second conversion efficiency, which constitutes more than two orders of magnitude improvement compared to the original experiments. A detailed discussion of these experiments and an analysis of time-to-space conversion using this technique are given in Section IV. In Section V, we conclude.

II. Pulse Shaping and Spectral Holography

A. Femtosecond Pulse Shaping

Fig. 1 shows the basic pulse-shaping apparatus, which we discuss briefly here. A more detailed description has been given in previous publications [1], [5], [6]. In pulse shaping, an ultrashort laser pulse is incident on a simple grating and lens apparatus, which spatially separates the pulse into individual optical frequency components. The lenses are identical and separated by twice their focal length; this forms a unit magnification telescope with the gratings placed at the outer focal planes of the lenses. Midway between the two lenses, where the spatial separation of the frequencies is a maximum, one can insert spatially patterned masks, or programmable spatial light modulators, in order to manipulate the amplitude and the phase of the spatially dispersed optical frequency components. After the various frequencies are reassembled into a single collimated beam, one obtains a shaped pulse, with the pulse shape determined by the Fourier transform of the amplitude and phase pattern imposed on the spectrum by the masks. The pulse shaper is dispersion free, so that in the absence of a mask, the output and input pulses are identical.

The first use of the pulse-shaping apparatus shown in Fig. 1 was reported by Froehly [7], who performed pulse-shaping experiments with input pulses 30 ps in duration. Related experiments demonstrating shaping of pulses a few picoseconds in duration by spatial masking within a fiber and grating pulse compressor were demonstrated independently by Heritage and Weiner [8], [9], [10]. The dispersion-free apparatus in Fig. 1 was subsequently adopted by Weiner *et al.* for manipulation of femtosecond optical pulses [5], [11]. With minor modifications, pulse-shaping operation has been successfully demonstrated for pulses below 20 fs in duration [12], [13]. The apparatus of Fig. 1 (without the mask) can also be used for pulse stretching or compression by changing the gratings-lens spacing. This idea was introduced and analyzed by Martinez [14] and is now used extensively in chirped pulse amplification.

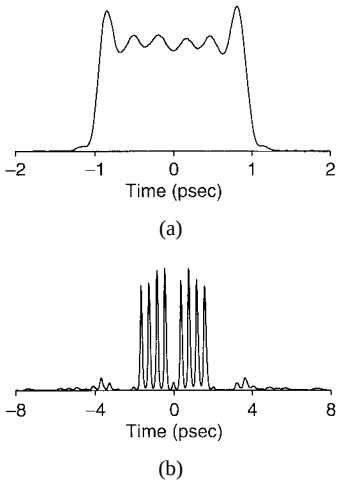

Fig. 2. Intensity cross-correlation traces of shaped pulses, measured using unshaped reference pulses directly from the laser. (a) Picosecond square pulsegenerated using microlithographically fabricated amplitude and phase masks. (b) Ultrafast optical pulse ("bit") sequence, generated using phase only filtering.

Fig. 2 shows of examples of shaped pulses generated using fixed masks. Fig. 2(a) shows a 2-ps square pulse with ∼100-fs transition times (comparable to the duration of the input laser pulses) [5]. This pulse was generated by using both phase and amplitude masks to pattern the spectrum according to a truncated sinc-function. Square pulses with flatter tops have also been demonstrated by appropriately apodizing the masking functions [15]. Fig. 2(b) shows an example of an ultrafast pulse sequence with an effective modulation rate of 2.5 THz [16]. Such sequences may be useful as ultrafast data packets for time-division multiplexed optical communications networks. It is interesting to note that the pulse sequence shown in Fig. 2(b) was generated with a phase mask only. In situations where only the time-domain intensity profile is specified, and the temporal phase is left as a free parameter [as in Fig. 2(b)], one can often design a phase-only filter to generate the desired intensity profile [16], [17]. This allows one to avoid the loss associated with amplitude filters. Phase-only filters have been extensively explored in spatial optics. The pulse sequence shown here was actually generated using a phase-only filter known as a Dammann grating, which was originally designed for generation of spot arrays for space-domain interconnect applications [18], [19].

The required spatial masking has been demonstrated using a number of technologies. The original work on femtosecond pulse shaping used microlithographically fabricated phase and amplitude masks, as above [5]. Currently, most attention is focused on programmable spatial light modulators that allow computer control over the masking pattern with millisecond reprogramming times. The first demonstrations of programmable pulse shaping used one-dimensional (1-D) liquid crystal phase modulator arrays with up to 128 modulator pixels and millisecond reprogramming times [6], [20]. Arrays allowing independent gray-level phase and amplitude control were subsequently developed [21] and are now available

commercially. Faster liquid crystal modulators allowing binary spectral phase modulation with 100-μs reprogramming times have also been reported [22]. Pulse shaping using an acoustooptic modulator as a programmable mask has also been demonstrated [23] and is seeing application with amplified femtosecond systems. Optoelectronic modulator arrays have potential to serve as pulse-shaping masks with subnanosecond reprogramming times appropriate for communications and information processing applications. The one experiment reported to date used an array of GaAs multiple quantum well modulators within a pulse-shaper setup to carve the input pulse spectrum into a number of separate wavelength channels for wavelength-division multiplexed (WDM) optical communications [24]. Application of optoelectronic modulator arrays for time-domain pulse-shaping applications has not yet been reported. Pulse shaping based on the use of spherical [25], moving [26] and deformable [27] mirrors and on holograms [28], [29], [30], [31], [32] has also been reported.

Pulse shaping has been or is currently being used in a number of laboratories for a broad range of applications, including coherent control over ultrafast physical processes, high field physics, ultrafast nonlinear optics in fibers, and high-speed information networks. A review of some of these applications is given in [1]. The pulse-shaping applications demonstrated by Weiner and coworkers include dark soliton propagation [33], [34] and enhanced nonlinear optical switching [15] in fibers, coherent control in solid-state materials [35], [36], and manipulation and enhancement of ultrafast terahertz radiation [37], [38].

There are a number of opportunities to apply pulse-shaping techniques in optical communications and, networking. We have already discussed in connection with Fig. 2(b) the possibility of generating ultrafast data packets for time-division multiplexed (TDM) communications. A new concept for processing of such packets is proposed in Section III. In WDM communications, the pulse-shaping technique allows realization of nearly arbitrarily programmable spectral filters, which can be used to construct WDM cross-connect switches with flat-topped frequency response [39], multichannel WDM gain equalizers [40], or hybrid WDM/space-division multiplexed optoelectronic switching systems [41]. Note that for these WDM applications, the input signal will usually consist of a series of mutually incoherent wavelength channels rather than a coherent pulse. Another application is for code-division multiple-access (CDMA) optical communications, in which different users sharing the fiber channel are distinguished on the basis of different minimally interfering optical codes. Here, pulse shaping can be used for either frequency-domain phase [42], [43], [44] or amplitude [45], [46] coding (and decoding). Optical CDMA based on spectral phase coding of femtosecond pulses is currently under investigation in our group at Purdue [47], [48]. Pulse shaping has also been used to correct for cubic (or higher order) phase distortion encountered for example in transmission of femtosecond pulses over kilometer lengths of fiber [49] and has been used inside a mode-locked external cavity diode laser to generate synchronized modelocked pulse trains simultaneously at several different wavelengths for hybrid TDM-WDM communications [50].

We have recently demonstrated two interesting extensions of pulse shaping. The first experiment demonstrates the use of a programmable pulse shaper for phase filtering of incoherent light from an erbium doped fiber amplified spontaneous emission source [51]. Related experiments were also reported in [52], [53]. Although the result of phase filtering of incoherent light is still incoherent light, nevertheless, the phase filtering operation does affect the electric field cross correlation function between the light before and after the pulse shaper. We have shown that the pulse shaper can manipulate this correlation function much in the same way that a pulse shaper can manipulate the output intensity profile for coherent input pulses. One motivation for performing this work is the possibility of using coherence coding of inexpensive incoherent light sources (instead of expensive femtosecond pulse sources) for certain classes of optical CDMA systems [45], [46], [52].

In a second recent experiment [54], [55], we have demonstrated a modified pulse shaper incorporating microlens arrays adjacent to the masking plane. The motivation for this work is the desire to demonstrate rapidly programmable pulse shaping using optoelectronic modulator arrays to perform the masking function. Typical optoelectronic arrays have large amounts of dead space between the active modulator elements. This would lead to distortion in standard pulse-shaping systems where the optical spectrum is spread along a continuous line in the pulse-shaping plane, since optical frequencies impinging on the dead spaces in the array would not be properly controlled. The microlens arrays in the modified pulse-shaper focus the optical frequency spectrum into a series of discrete spots which should better match the format of an optoelectronic modulator array.

At this point we give a very brief theoretical description [1], [56] of pulse shaping. Since the pulse-shaping apparatus acts as a linear filter for femtosecond input pulses, its response can be characterized in the frequency domain by

$$E_{\rm out}(\omega) = E_{\rm in}(\omega)H(\omega) \tag{1}$$

where $E_{\rm in}(\omega)$ and $E_{\rm out}(\omega)$ are the Fourier transforms of the input and output electric fields, respectively, and $H(\omega)$ is the complex frequency response of the linear filter acting on the femtosecond pulses. We wish to relate $H(\omega)$ to the actual physical masking function with complex transmittance $M(x)$. To do so, we note that the field immediately after the mask can be written

$$E_m(x,\omega) \sim E_{\rm in}(\omega)e^{-(x-\alpha\omega)^2/w_o^2}M(x) \tag{2}$$

where

$$\alpha = \frac{\lambda^2 f}{2\pi c d\cos(\theta_d)} \tag{3a}$$

and

$$w_o = \frac{\cos(\theta_{\rm in})}{\cos(\theta_d)}\left(\frac{f\lambda}{\pi w_{\rm in}}\right). \tag{3b}$$

Here α is the spatial dispersion with units cm (rad/s)$^{-1}$, w_o is the radius of the focused beam at the masking plane (for any single frequency component), $w_{\rm in}$ is the input beam radius before the first grating, c is the speed of light, d is the grating

period, λ is the wavelength, f is the lens focal length, and θ_{in} and θ_d are the input and diffracted angles from the first grating, respectively.

Note that (2) is a function of both space (x) and frequency (ω). This occurs because the spatial profiles of the focused spectral components can be altered by the mask, e.g., some spectral components may impinge on abrupt amplitude or phase steps on the mask, while others may not. This leads to different amounts of diffraction for different spectral components and results in an output field that may be a complicated function of space and time. This space–time coupling has been analyzed by several authors [57]–[59].

On the other hand, one is usually interested in generating a spatially uniform output beam with a single prescribed temporal profile. In order to obtain an output field which is a function of frequency (or time) only, one must perform an appropriate spatial filtering operation. Thurston *et al.* [56] analyze pulse shaping by expanding the masked field (2) into Hermite–Gaussian modes and assuming that all of the spatial modes except for the fundamental Gaussian mode are eliminated by the spatial filtering. In real experiments the Gaussian mode selection operation could be performed by focusing into a fiber (for communications applications) or by coupling into a regenerative amplifier (for high-power applications). This can be also be performed approximately by spatial filtering or simply by placing an iris after the pulse-shaping setup. In any case, if one takes the filter function $H(\omega)$ to be the coefficient of the lowest Hermite–Gaussian mode in the expansion of $E_m(x,\omega)$, one arrives at the following expression [1], [56]:

$$H(\omega) = \left(\frac{2}{\pi w_o^2}\right)^{1/2} \int dx M(x) e^{-2(x-\alpha\omega)^2/w_o^2}. \quad (4)$$

Equation (4) shows that the effective filter in the frequency domain is the mask function $M(x)$ convolved with the *intensity* profile of the beam. The main effect of this convolution is to limit the full-width at half-maximum (FWHM) spectral resolution $\delta\omega$ of the pulse shaper to $\delta\omega \cong (\ln 2)^{1/2} w_o/\alpha$. Physical features on the mask smaller than $\sim w_o$ are smeared out by the convolution, and this limits the finest features which can be transferred onto the filtered spectrum. One consequence of this picture is that wavelength components impinging on mask features which vary too fast for the available spectral resolution are in part diffracted out of the main beam and eliminated by the spatial filter. This can lead to phase-to-amplitude conversion in the pulse-shaping process. Conversely, in the limit $w_o \to 0$, the apparatus provides perfect spectral resolution, and the effective filter is just a scaled version of the mask.

Note that in our treatment above we assume that the output Gaussian mode which is selected is matched to the input mode. The case where the input and output mode sizes are not matched is analyzed in [60]; in some cases this can give improvement in spectral resolution compared to that expected from (4).

The effect of finite-spectral resolution can be understood in the time domain by noting that the output pulse $e_{\text{out}}(t)$ will be the convolution of the input pulse $e_{\text{in}}(t)$ with the impulse response $h(t)$. The impulse response in turn is obtained from the Fourier transform of (4) and can be written as follows:

$$h(t) = m(t)g(t) \quad (5a)$$

where

$$m(t) = \frac{1}{2\pi} \int d\omega M(\alpha\omega) e^{i\omega t} \quad (5b)$$

and

$$g(t) = \exp\left(-w_o^2 t^2/8\alpha^2\right). \quad (5c)$$

Thus, the impulse response is the product of two factors. The first factor $m(t)$ is the Fourier transform of the mask (appropriately scaled) and corresponds to the infinite-resolution impulse response. The second factor $g(t)$ is an envelope function that restricts the time window in which the tailored output pulse can accurately reflect the response of the infinite-resolution mask. The full-width half-maximum duration of this time window (in terms of intensity) is given by

$$\text{FWHM}_t = \frac{4\alpha\sqrt{\ln 2}}{w_o} = \frac{2\sqrt{\ln 2} w_{\text{in}} \lambda}{cd\ \cos\theta_{\text{in}}}. \quad (6)$$

The time window is proportional to the number of grating lines illuminated by the input beam multiplied by the period of an optical cycle. A larger time window can only be obtained by expanding the input beam diameter. The shortest feature in the output shaped pulse is of course governed by the available optical bandwidth.

Equations (4) and (5), which result from an approximate treatment of diffraction at the mask, have been found to adequately describe a great number of experimental situations. Experiments show that both the available time window and the available frequency resolution are well modeled. We reiterate, however, that these results are valid only when a suitable spatial filter is employed so that the pulse shape is constant across the spatial beam profile. Practically, it is also helpful to avoid using a masking function whose infinite resolution impulse response function (5b) significantly exceeds the available time window (5a).

B. Spectral Holography

Further pulse processing capabilities are achieved through an extension of pulse shaping called spectral holography [29], [61], in which the pulse-shaping mask is replaced by a holographic or nonlinear material. Spectral holography was first proposed theoretically [61] in the Russian literature, and subsequent experiments demonstrating the principles of time-domain processing via spectral holography were performed by Weiner [29]. In analogy with off-axis spatial holography, two beams are incident: an unshaped femtosecond reference pulse with a uniform spectrum, and a temporally shaped signal waveform with information patterned onto the spectrum. The spectral components making up the reference and signal pulses are spatially dispersed and interfere at the Fourier plane. The resulting fringe pattern is stored by using a holographic recording medium. During readout with a short test pulse, each spectral component from the test pulse diffracts off that part

of the hologram containing phase and amplitude information corresponding to the same frequency component from the signal beam. The diffracted frequencies are then recombined into a pair of output beams, corresponding to $+1$ and -1 order diffraction, respectively. Assuming linear holographic recording and sufficient spectral resolution, the reconstructed field $E_{\text{out}}(\omega)$ can be written as follows:

$$E_{\text{out}}(\omega) \sim E_t(\omega)E_r^*(\omega)E_s(\omega)e^{i\bar{K}_1\cdot\bar{r}} + E_t(\omega)E_r(\omega)E_s^*(\omega)e^{i\bar{K}_2\cdot\bar{r}}. \quad (7)$$

Here, $E_t(\omega)$, $E_r(\omega)$, and $E_s(\omega)$ are the complex spectral amplitudes of the test, reference, and signal fields, respectively, and $\bar{K}_1$ and $\bar{K}_2$ are the propagation vectors of the diffracted output beams. The envelopes of the reconstructed output pulses are given by the Fourier transform of (7), as follows:

$$e_{\text{out}}(t) \sim e_t(t) * e_r(-t) * e_s(t)e^{i\bar{K}_1\cdot\bar{r}} + e_t(t) * e_r(t) * e_s(-t)e^{i\bar{K}_2\cdot\bar{r}}. \quad (8)$$

When both test and reference beams consist of unshaped pulses with durations short compared to the duration of the shaped signal pulse, the output pulse is either a real or a time-reversed reconstruction of the original signal pulse, depending on the diffraction direction. Furthermore, if the test beam itself is a shaped pulse, then one can generate the convolution or the correlation of the signal and test electric field envelopes. In the special case where the test and signal waveforms are identical, the correlation becomes a matched filtering operation, which is useful for chirp compensation and pulse compression and for ultrafast pattern matching.

Experiments demonstrating spectral holography in the ultrafast time domain were performed by Weiner using femtosecond, visible wavelength pulses [29], [62], [63]. The holographic material was a thermoplastic plate, which was first exposed to the signal-reference interference pattern and then "developed" to form a permanent spectral hologram. All of the signal processing operations enumerated above were successfully demonstrated. As one example, Fig. 3 shows data corresponding to matched filtering operation. All the data correspond to intensity cross-correlation measurements of output pulses resulting from the spectral holography process. The short output pulse shown in Fig. 3(a) results when all three pulses (signal, reference, and test) are ultrashort pulses with no distortion. In Fig. 3(b), pulse shaping is used to encode the signal pulse only into a low intensity pseudonoise burst similar to a spread-spectrum waveform. Finally, in Fig. 3(c), both signal and test pulses are encoded in the same way; the identical distortions cancel, and an intense bandwidth-limited output pulse is restored. These data illustrate the coding–decoding process that forms the basis for femtosecond code-division multiple-access (CDMA) communications. It is worth noting that such holographic matched filtering is a self-aligned process, so that one can decode or process incoming signals without having to precisely specify those signals beforehand.

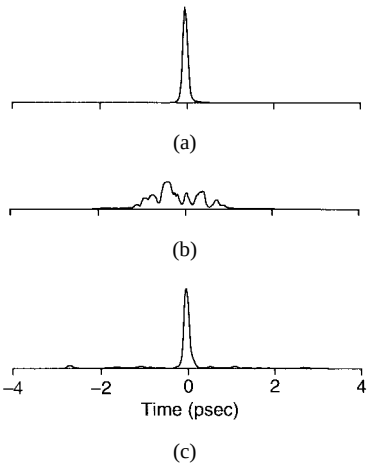

Fig. 3. Holographic matched filtering of coded ultrafast waveforms. (a) None of pulses are coded. (b) The signal is coded using pulse shaping. (c) Both signal and test pulses are coded, resulting in matched filtering operation and a restored output pulse.

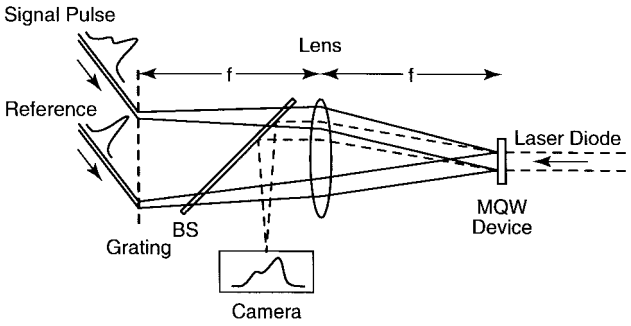

Fig. 4. Apparatus for space-to-time mapping using spectral holography and dynamic semiconductor photorefractive films [67].

C. Holographic Time–Space Conversion

In the previous section on spectral holography we discussed pure time-domain systems, in which an ultrafast input temporal signal is processed to yield a new output temporal signal. One can also consider hybrid spectral holography systems in which time and space are mixed. These systems allow conversion from the spatial domain into the ultrafast time domain (parallel to serial conversion) or from the ultrafast time domain into the spatial domain (serial to parallel conversion). Such hybrid space–time conversions have been discussed theoretically by Mazurenko [61], [64] and demonstrated experimentally by several groups [28], [65]–[68].

Time-to-space mapping of femtosecond optical waveforms can be achieved by recording a spectral hologram using time-domain signal and reference pulses, as in the previous section, and then reading out using a monochromatic, continuous-wave (CW) laser. Nuss [67] used the arrangement sketched in Fig. 4 for experiments demonstrating such time-to-space mapping. Femtosecond signal and reference pulses at $\sim$830 nm are obtained from a mode-locked Ti:sapphire laser, and a photorefractive multiple-quantum-well device (PRQW) [69], [70] is used as a dynamic holographic recording material. Key features of these PRQW's are a response time of ~ 1 μs at an intensity of 10 mW/cm^2 and a diffraction efficiency of a few

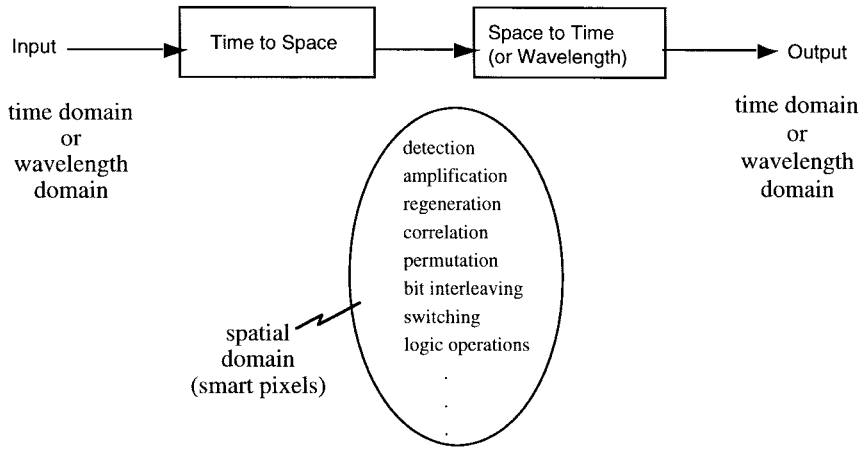

Fig. 5. Block diagram of generalized space–time pulse processing systems. By converting interchangeably between time, space, and wavelength domains, sophisticated data manipulation applications may be possible.

percent. Read-out is accomplished by using an 850-nm CW laser diode. By passing the diffracted output beam through a Fourier transform lens, the original temporal information is converted into spatial information. The spatial profile of the resulting output beam is given by the electric field cross-correlation between signal and reference pulses. For a short bandwidth limited reference pulse, this yields a spatial replica of the electric field amplitude of the original time-domain signal pulse.

In addition to PRQW's, bulk holographic crystals have also been employed for time-to-space conversion experiments [68]. However, both PRQW's and bulk holographic materials are too slow for use in most communication applications requiring gigabit per second frame rates. A related technique for time-to-space conversion of picosecond pulses was demonstrated by Ema, who utilized the exciton resonance in ZnSe for the nonlinearity required for holography [65]. Although this material has the advantage of fast response ($\sim$13 ps), its operation wavelength is 442 nm and it must be cooled to cryogenic temperatures. A third scheme, first demonstrated by Mazurenko, Fainman, and coworkers [2], [3], relies on the instantaneous nonlinear effect of SHG using a nonlinear optical crystal within a pulse shaper. This scheme is an important advance due to the combination of fast response and operation at convenient wavelengths and temperatures. We have performed similar time-to-space mapping experiments in which we demonstrate SHG conversion efficiencies above 50%. This work is described in detail in Section IV.

Finally, we note that spectral holography can also be utilized for the converse operation, namely, space-to-time conversion [28], [31], [32], [68]. Here one records a hologram of a one-dimensional spatial image onto a holographic recording material placed inside a pulse shaper. The hologram acts as a diffractive pulse-shaping mask and generates an output pulse which is a scaled version of the direct spatial image, or its Fourier transform, depending on the hologram recording geometry. In addition, by utilizing nonlinearities in the recording process, one can demonstrate new pulse processing operations, such as edge enhancement in space-to-time conversion [32].

III. Generalized Time–Space Systems for Ultrahigh-Speed Data Processing

By exploiting the ability to convert between space and time in pulse shaping and spectral holography, one can envision new opportunities for data processing and manipulation of extremely broadband optical signals. Consider cascaded time–space systems as shown conceptually in Fig. 5. Here, an ultrafast time-domain data stream (or possibly a multiwavelength data signal) would first be converted into the space-domain. Various processing operations could then be performed using high speed smart pixel optoelectronic arrays. The smart pixel array would include detectors for reading the space-domain data, VLSI electronics for processing, and modulators for converting back to the ultrafast time (or the wavelength) domain using an appropriate pulse-shaping setup. Experiments demonstrating cascaded space-to-time and time-to-space conversion based on spectral holography were reported previously [68], but no further processing was performed. The combination of time–space conversions and space-domain (parallel) optoelectronic processing could lead to great flexibility for implementing new types of ultrafast optical data processing.

Key to this concept is the use of arrays of optoelectronic "smart pixels" to implement the spatial-domain processing function. Smart pixel device arrays, in which optoelectronic transceivers such as detectors and modulators are intimately coupled to electronic processing circuitry at every pixel of the array, have recently emerged as a key technology for traditional (i.e., spatial domain) optical signal processing systems and optical interconnect systems [71], [72]. The main theme is to build systems in which optics and electronics can each perform the functions for which they are most ideally suited. Here, our aim is to employ smart pixel technology in an application for which it has previously received little attention—namely, for manipulation and processing of ultrafast time-domain optical signals. By incorporating high performance smart pixel device arrays into ultrafast pulse processing systems, we can accelerate processing times substantially and achieve completely new functionalities.

As a demonstration vehicle, we have initiated experiments using the hybrid SEED smart pixel technology [73], which is available through Bell Laboratories on a foundry basis. This technology consists of arrays of gallium arsenide multiple quantum well (GaAs MQW) optical detectors/modulators, or SEED's, bonded onto the surface of silicon CMOS (Si-CMOS) electronic chips, forming smart pixel arrays. The CMOS circuitry is custom designed in order to implement the desired processing functionalities. This technology can be expected to operate with frame rates up to the gigabit-per-second range, depending on the minimum feature size of the particular CMOS process employed. Our current experiments are being performed using pulses from a modelocked Ti:sapphire laser in order to match the ~850-nm operating wavelength of the hybrid SEED optoelectronics. For actual communications experiments, one would likely need to operate in the 1.5-μm band. This could potentially be achieved by fabricating smart pixel arrays based on asymmetric Fabry–Perot modulators (AFPM's). Although AFPM's and AFPM arrays were initially developed in the 850-nm spectral region [74]–[76], single device operation was recently extended to the 1.5-μm band with both very high speed (>20 Gb/s) and high on-off contrast (>15 dB) in a format compatible with array operation [77]. Alternatively, for some applications one may be able to exploit the wavelength conversion inherent in SHG time-to-space conversion to match a 1.5-μm operating wavelength to 850 nm GaAs optoelectronics.

As illustrated in Fig. 5, the use of smart pixel optoelectronics could potentially allow tailoring of a wide range of system functionalities through the VLSI design. Examples include data detection and regeneration, time-slot interchanging, digital optical gating, packet header recognition, and TDM–WDM data format conversion. With suitable optoelectronics and materials, it may be feasible, for example, to implement such functionalities for 100-Gb/s time-division multiplexed optical data, by using 32-element smart pixel arrays operating in parallel at 3.2-Gb/s frame rates. Such a combination of functionality and speed is not currently available through any established technology.

IV. Time-to-Space Conversion Using Second-Harmonic Generation

A. Overview and Experimental Setup

As noted earlier, a scheme for time-to-space conversion based on SHG within a pulse shaper was recently demonstrated by Mazurenko, Fainman, and coworkers [2], [3]. Since the SHG nonlinearity is essentially instantaneous, this work is an important advance compared to previous time-to-space conversion methods which depended on materials with slower nonlinear responses. However, in previous short pulse experiments where SHG was performed using angle-tuned type-I phase matching in an LBO crystal [3], the conversion efficiency was rather low (~0.1%). We have recently achieved femtosecond optical time-to-space mapping with more than 50% conversion efficiency using temperature-tuned noncritical phase matching (NCPM) in a thick $KNbO_3$ nonlinear crystal. This increase in efficiency by more than 500 fold may enable systems using time-to-space mapping in conjunction with smart pixel optoelectronic device arrays to perform sophisticated ultrafast pulse processing operations repeatable at communication rates with realistic power budgets.

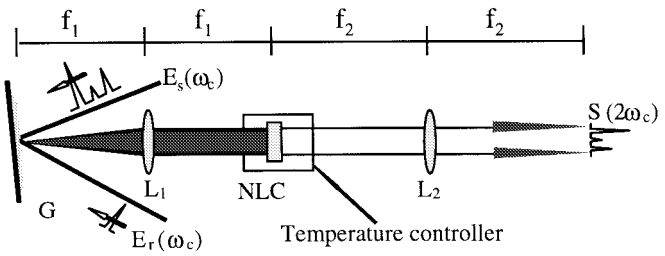

Fig. 6. Schematic diagram of time-to-space conversion apparatus using SHG within a femtosecond pulse shaper. G: Grating. L_1, L_2: lenses. E_s: Signal beam. E_r: Reference beam. NLC: Potassium niobate nonlinear crystal.

In the rest of this paper, we discuss our time-to-space conversion experiments using $KNbO_3$. We first describe the experimental setup. We then analyze the time-to-space mapping operation theoretically, pointing out similarities to pulse shaping throughout. Finally, we present our experimental results validating the theory and demonstrating the >50% conversion efficiency in time-to-space mapping. The analysis of the conversion efficiency itself is being published elsewhere [4] and is not repeated here.

The experimental arrangement, which is similar to that in [3], is shown in Fig. 6. A short pulse (~125 fs FWHM) emitted by a mode-locked Ti-sapphire oscillator is split into two beams, a featureless reference pulse $e_r(t)$ and a signal beam, $e_s(t)$, which can be shaped. The two beams are diffracted by the single diffraction grating (600 lines/mm) such that the $+1$ diffraction order from one beam overlaps with the -1 order from the other. The two diffracted beams pass through lens L_1 (focal length 6 cm) and are spectrally dispersed in the back Fourier plane of the lens. We have utilized both a collinear as well as a noncollinear geometry, in which the two beams are displaced vertically by a few mm at the grating. The two beams interact in the $KNbO_3$ nonlinear crystal that is mounted on a thermoelectric (TE) cooler for precise temperature control. Since the spatial dispersions of the two beams are equal in amplitude and opposite in sign, the spot with frequency $\omega_o + \Delta\omega$ from the signal beam spatially overlaps and mixes with the spot with frequency $\omega_o - \Delta\omega$ from the reference beam. This interaction in a nonlinear crystal while satisfying the phase matching condition results in generation of a blue SHG beam that oscillates at the optical frequency $2\omega_o$ and is quasi-monochromatic. For a sufficiently short reference pulse, the spatial profile of the blue beam at the output of the crystal is the Fourier transform of $e_s(t)$. By performing a spatial Fourier transform using lens L_2 (with focal length $f_2 = 16$ cm), a spatial replica of $e_s(t)$ is obtained and recorded using a charge-coupled device (CCD) camera.

In order to illustrate the spatial dispersion within the pulse shaper, in Fig. 7, we have plotted data on peak wavelength as a function of transverse position in the plane of the nonlinear crystal for both reference and signal beams. These data were measured by placing an optical fiber connected to an optical

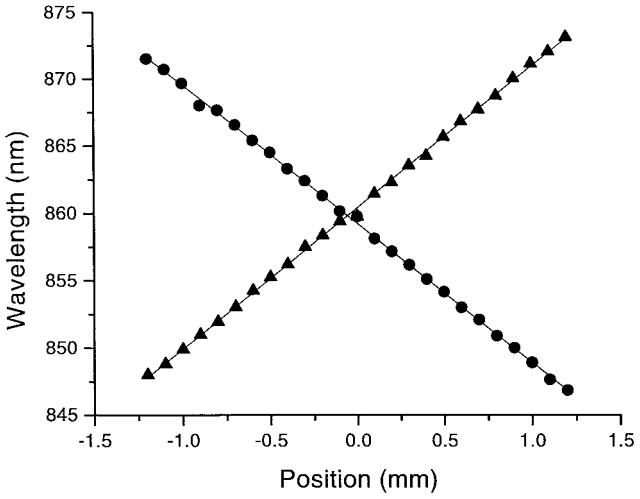

Fig. 7. Plot of wavelength as a function of transverse position at the pulse-shaper masking plane for signal and reference beams. The two beams have equal but opposite spatial dispersions.

spectrum analyzer into the spectrally dispersed beams. By translating the fiber in the spectral dispersion direction, we were able to record the spatially dependent spectra. From Fig. 7, we see that the wavelength corresponding to the peak of the spectrum varies linearly with position. A linear fit to the data yields a variation of 10.488 nm/mm for the signal beam and -10.40 nm/mm for the reference beam. The slopes are nearly equal and opposite, as required for this time-to-space conversion scheme.

Our experiments are performed using a $5 \times 3 \times 6.2$ mm a-cut $KNbO_3$ crystal. $KNbO_3$, a biaxial crystal that belongs to space group *Bmm2*, is known to possess high nonlinear coefficient ($d_{32} \sim 20$ pm/V) [78]. In addition to its good optical quality and large damage threshold [79], $KNbO_3$ allows noncritical type I phase matching for blue generation at around 430 nm by temperature tuning. These properties make this crystal an attractive choice for our application. Because of its large group velocity mismatch ($\sim$1.2 ps/mm for 860–430-nm conversion [80]) and narrow phase matching bandwidth ($\sim$0.07 nm for crystal length of 6.2 mm), this crystal has been useful mainly for doubling CW and to some extent picosecond pulsed lasers. It is usually avoided for femtosecond applications. Since our experiment converts femtosecond input pulses into quasi-monochromatic upconverted pulses, the narrow phase matching bandwidth is not a serious limitation. This opens up the use of the large nonlinear coefficient in a noncritically phase-matched geometry with no spatial walkoff to allow high conversion efficiency and is an important contribution of our work. In our experiments, the fundamental beam propagates along the crystallographic a-axis with its polarization along the b-axis generating a nonlinear polarization $P(2\omega)$ with second-harmonic beam polarized along the c-axis (using the nonlinear coefficient d_{32}). In this case, the fundamental wavelength can be tuned between 840 and 940 nm for temperatures between -38 °C and 180 °C [81]. Here, we tune the center wavelength of the laser to 857.7 nm which allows type-I NCPM for the quasi-monochromatic output at 428.85 nm at room temperature.

In the following, we first describe the theory of time-to-space conversion via SHG in a pulse shaper. We then proceed to discuss the experimental results.

B. Time-to-Space Conversion Theory

A theory for time-to-space conversion using spectral SHG was previously published by Sun, Mazurenko, and Fainman [3]. Here, we sketch a theory which follows a similar line, but with some differences as well. These include the following:

(1) We include the effects of group velocity walkoff and finite phase matching bandwidth in the nonlinear crystal. This is especially relevant for our experiments using a thick nonlinear crystal and allows us to predict the temperature tuning response of the nonlinear crystal inside the pulse shaper.
(2) We specialize to the practically important case of Gaussian input beams, which simplifies the calculations and leads to additional physical insight.
(3) We specifically relate the time window and other features of signals produced in time-to-space conversion to the relevant concepts that have previously been developed in the context of pulse shaping.

We have previously analyzed the conversion efficiency in SHG-based time-to-space converters and discussed how to achieve high efficiency [4]. Since this analysis is given elsewhere, it is not repeated here.

For our calculations we assume input signal and reference fields, $e_s(t)$ and $e_r(t)$ respectively, as follows:

$$e_s(x,t) = \mathrm{Re}\big[a_s(t)e^{-x^2/w_{\mathrm{in}}^2}e^{j\omega_o t}\big] \tag{9a}$$

$$e_r(x,t) = \mathrm{Re}\big[a_r(t)e^{-x^2/w_{\mathrm{in}}^2}e^{j\omega_o t}\big]. \tag{9b}$$

Here $a_s(t)$ and $a_r(t)$ are the slowly varying complex electric field envelope functions, ω_o is the center frequency of the input pulses, and Gaussian beams with radius w_{in} are assumed. We take x to represent the transverse dimension in which the frequencies are spatially dispersed. One would usually assume a Gaussian variation in the second transverse direction (y) as well; however, since there is no spectral dispersion in this direction, the y spatial variation has no effect on the time-to-space conversion operation and is therefore omitted in our analysis. The Fourier transform of the signal pulse envelope function is given by

$$A_s(\omega) = \int dt\; a_s(t)e^{-j\omega t} \tag{10}$$

with a similar expression for $A_r(\omega)$.

The optical frequency components are spatially dispersed by the grating and first lens with focal length f_1. Following standard pulse-shaping analysis [1], [14], [56], [82] the signal field $e_s'(x,t)$ in the Fourier plane of L_1 is given by e6

$$e_s'(x,t) = \mathrm{Re}\left[\frac{1}{2\pi}e^{j\omega_o t}\int d\omega e^{j\omega t}A_s(\omega)e^{-(x-\alpha\omega)^2/w_o^2}\right]. \tag{11}$$

The spatial dispersion parameter α and focused spot size in the Fourier plane w_o are given by (3a), (3b). The spatial dispersion of the reference field is assumed to be equal and opposite to

that of the signal field. Therefore, we have

$$e'_r(x,t) = \mathrm{Re}\left[\frac{1}{2\pi} e^{j\omega_o t} \int d\omega e^{j\omega t} A_r(\omega) e^{-(x+\alpha\omega)^2/w_o^2}\right]. \quad (12)$$

The nonlinear polarization responsible for time-to-space conversion depends on the product of signal and reference fields. We ignore the self-terms due to the reference and signal fields individually since: 1) these terms do not result in time-to-space conversion; 2) these terms are not phase matched except for frequencies very close to ω_o; and (3) these terms can be eliminated by using a noncollinear beam geometry. The component of the nonlinear polarization oscillating near the second-harmonic frequency $2\omega_o$ is written

$$P_{\mathrm{NL}}(x,t) \sim \mathrm{Re}\left[\frac{1}{(2\pi)^2} e^{2j\omega_o t} \int d\omega_1 e^{j\omega_1 t} A_s(\omega_1) e^{-(x-\alpha\omega_1)^2/w_o^2} \cdot \int d\omega_2 e^{j\omega_2 t} A_r(\omega_2) e^{-(x+\alpha\omega_2)^2/w_o^2}\right]. \quad (13)$$

Here, we have assumed that depth of focus is sufficiently long that the beam radius does not vary appreciably within the nonlinear crystal, an approximation that is only partly true in our experiments. However, since most of the second harmonic is generated near the beam waist, this approximation is expected nevertheless to yield reasonable results. We now introduce the frequency variable $\Omega = \omega_1 + \omega_2$, which physically signifies an actual second-harmonic frequency at $2\omega_o + \Omega$. Substituting in for ω_2 and combining all the Gaussian terms, one obtains

$$P_{\mathrm{NL}}(x,t) \sim \mathrm{Re}\left[\left(\frac{1}{2\pi}\right)^2 e^{2j\omega_o t} \int d\Omega e^{j\Omega t} e^{-\frac{1}{2}(\alpha\Omega/w_o)^2} \cdot \int d\omega_1 A_s(\omega_1) A_r(\Omega-\omega_1) e^{-2[x+\frac{\alpha}{2}(\Omega-2\omega_1)]^2/w_o^2}\right]. \quad (14)$$

In the undepleted pump approximation, the generated second-harmonic field $e'_{\mathrm{SHG}}(x,t)$ at the output of the nonlinear crystal is simply proportional to $P_{\mathrm{NL}}(x,t)$, assuming broadband phase matching. The case of finite phase matching bandwidth is handled by multiplying by an additional filtering function $H_{\mathrm{PM}}(\Omega)$ that acts only on the second-harmonic frequency parameter Ω. As is well known [83]–[85], the finite-phase-matching bandwidth arises due to group velocity walkoff between the fundamental and second-harmonic fields, where the bandwidth within which second harmonic can be efficiently generated is inversely proportional to the group velocity walkoff. The generated field after the nonlinear crystal is then written as

$$e'_{\mathrm{SHG}}(x,t) \sim \mathrm{Re}\left[\left(\frac{1}{2\pi}\right)^2 e^{2j\omega_o t} \int d\Omega e^{-\frac{1}{2}(\alpha\Omega/w_o)^2} H_{\mathrm{PM}}(\Omega) \cdot \int d\omega_1 A_s(\omega_1) A_r(\Omega-\omega_1) e^{-2[x+\frac{\alpha}{2}[\Omega-2\omega_1]^2/w_o^2]}\right]. \quad (15)$$

Finally, the output field $e''_{\mathrm{SHG}}(x,t)$ in the back Fourier plane of lens L_2 is obtained by performing a spatial Fourier transform [86]:

$$e''_{\mathrm{SHG}}(x,t) = \int dx' e'_{\mathrm{SHG}}(x',t) e^{-j\beta x x'} \quad (16)$$

where $\beta = \frac{2\omega_o}{cf_2}$ is the Fourier transform scale factor. The result is

$$e''_{\mathrm{SHG}}(x,t) \sim \mathrm{Re}\left[\left(\frac{1}{2\pi}\right)^2 e^{2j\omega_o t} e^{-\frac{1}{8}(\beta w_o x)^2} \cdot \int d\Omega e^{j\Omega(t+\frac{\alpha\beta x}{2})} e^{-\frac{1}{2}\left(\frac{\alpha\Omega}{w_o}\right)^2} H_{\mathrm{PM}}(\Omega) \cdot \int d\omega_1 e^{-j\alpha\beta x\omega_1} A_s(\omega_1) A_r(\Omega-\omega_1)\right]. \quad (17)$$

We now make the simplifying assumption that $A_r(\Omega-\omega_1) \approx A_r(-\omega_1)$. This is valid provided that the reference spectrum does not vary significantly within the spectral resolution of the pulse shaper, i.e., within the range of physically overlapping frequencies present at any single position x at the nonlinear crystal. We do not place any such restriction on the signal spectrum. We can then rewrite the output field as

$$e''_{\mathrm{SHG}}(x,t) \sim \mathrm{Re}\left[\left(\frac{1}{2\pi}\right)^2 e^{2j\omega_o t} B(x) C(x,t) D(x)\right] \quad (18a)$$

where

$$B(x) = e^{-\frac{1}{8}(\beta w_o x)^2} \quad (18b)$$

$$C(x,t) = \int d\Omega e^{j\Omega(t+\alpha\frac{\beta}{2}x)} e^{-\frac{1}{2}(\frac{\alpha\Omega}{w_o})^2} H_{\mathrm{pm}}(\Omega) \quad (18c)$$

$$D(x) = \int d\omega_1 e^{-j\alpha\beta x\omega_1} A_s(\omega_1) A_r(-\omega_1). \quad (18d)$$

Physically, $B(x)$, $C(x,t)$, and $D(x)$ represent the finite-spatial (or temporal) window for time-to-space conversion, the temporal output waveform, and the time-to-space mapping function, respectively. Each term is discussed in further depth below.

Let us first discuss the time-to-space mapping function $D(x)$, which is the Fourier transform of $A_s(\omega_1)A_r(-\omega_1)$. Evaluating the transform yields

$$D(x) = \int a_s(\alpha\beta x') a_r(\alpha\beta(x'+x))\, dx'. \quad (19)$$

The output field is a spatial replica of the cross correlation of the signal and reference field envelopes. It is important to note that neither field is complex conjugated, unlike the usual case of electric field correlations obtained, e.g., by using an interferometer. In the limit where $a_r(t)$ is much shorter than $a_s(t)$, the spatial profile of the output electric field is proportional to $a_s(\alpha\beta x)$. Thus, the time-to-space mapping function can be written

$$t \leftrightarrow \alpha\beta x \quad (20a)$$

$$x \leftrightarrow (\alpha\beta)^{-1} t \quad (20b)$$

where

$$(\alpha\beta)^{-1} = \left(\frac{f_2}{f_1}\right)\left(\frac{\omega_o}{2\omega_o}\right)\left(\frac{cd\ \cos\theta_d}{\lambda}\right) = \left(\frac{f_2}{f_1}\right)\left(\frac{cd\ \cos\theta_d}{2\lambda}\right). \quad (20c)$$

$(\alpha\beta)^{-1}$ is the time-to-space conversion factor, with units meters per second. This expression is the same as that described for the case of time-to-space transformation using a thin photorefractive film [67] except for a factor of 1/2, which arises due to the difference in input and output frequencies (ω_o and $2\omega_o$).

Note also that the output field profile depends only on the relative timing of the signal and reference pulses, not on the absolute timing of either field. Common mode timing shifts of both fields do not lead to any shifts in the output spatial pattern. This is one simple manifestation of the correlation operation expressed by (19). One can also perform experiments where the reference pulse is itself patterned in time. In this case the output spatial profile is the correlation of the two input temporal waveforms.

We next discuss the spatial window function $B(x)$. Clearly, this function reduces the intensity of the output image as x becomes too large. Since there is a linear mapping between x and t, this means that there is a limited time window (centered on the reference pulse) within which the signal pulse can be imaged. The full-width at half-maximum of the output spatial intensity is given by

$$\mathrm{FWHM}_x = \frac{4\sqrt{\ln 2}}{\beta w_o} = \frac{\sqrt{\ln 2} f_2 w_{\mathrm{in}} \cos\theta_d}{f_1 \cos\theta_{\mathrm{in}}}. \quad (21)$$

The equivalent intensity full-width maximum time window is given by

$$\mathrm{FWHM}_t = \frac{4\alpha\sqrt{\ln 2}}{w_o} = \frac{2\sqrt{\ln 2} w_{\mathrm{in}} \lambda}{cd\cos\theta_{\mathrm{in}}}. \quad (22)$$

Physically, we can understand this windowing effect as follows. At any physical location x at the nonlinear crystal, there coexists a range of frequencies $\Delta\nu \approx w_o/2\pi\alpha$. The SHG at a single spot at the crystal results from an integration over all the frequencies contributing to that spot. As long as the signal spectrum is smooth on the scale of $\Delta\nu$, this does not affect the generated second-harmonic field (we have already assumed earlier in our derivation that the reference spectrum is smooth on the scale of $\Delta\nu$). However, if the spectrum does vary significantly within this $\Delta\omega$, then that variation is smoothed out by the averaging over a finite range of frequencies. This determines the minimum-sized feature in the frequency domain, which can accurately be converted into a second-harmonic spatial pattern at the nonlinear crystal. It is worth noting that the time window formula, (22), is exactly the same as the window obtained in the analysis of pulse shaping (6).

We now comment on the term $C(x,t)$. Since the output image will usually be detected by a time-integrating detector array, the detected signal will be proportional to

$$\int |e''_{\mathrm{SGH}}(x,t)|^2\, dt \sim |B(x)D(x)|^2 \int |C(x,t)|^2\, dt. \quad (23)$$

From Parseval's theorem, we can write

$$\int |C(x,t)|^2\, dt \sim \int e^{-(\alpha\Omega/w_o)^2} |H_{\mathrm{PM}}(\Omega)|^2\, d\Omega. \quad (24)$$

This is independent of both x and t, and therefore, has no effect on the detected image.

From this, we see that a finite phase matching bandwidth (and hence a finite-group velocity walkoff) does not influence the form of the detected image, since the x-dependence of the time integrated intensity is unaffected by the $H_{\mathrm{PM}}(\Omega)$ term. However, this term does affect the overall amplitude of the image and dictates the phase matching response in the time-to-space geometry. We return to this point later when we discuss the temperature tuning bandwidth of our experiments.

Finally, we comment on the time behavior of the output image as determined by $C(x,t)$. For infinite phase matching bandwidth, $H_{\mathrm{PM}}(\Omega) = 1$, the output is a Gaussian pulse with an intensity FWHM duration equal to one half of the time window given by (22). This pulse duration is again determined by the spectral resolution of the apparatus, which also determines the bandwidth of the quasi-monochromatic output image. A restricted phase matching range narrows the bandwidth and broadens the duration of the output pulse. In addition, the pulse has a position dependent delay equal to $-\alpha\beta x/2$. The ratio of the delay to the spatial coordinate (x) is equal to one-half of the time-to-space mapping constant $\alpha\beta$. Once again, this is similar to a phenomenon arising in pulse shaping, namely, in the absence of output spatial filtering, the pulse-shaping temporal window is offset from $t = 0$ by an amount proportional to the spatial offset (x) [58].

C. Time-to-Space Conversion Experimental Results

We now report experimental results for the setup discussed in Section III–A. The key parameters for these experiments are: $f_1 = 6$ cm, $f_2 = 16$ cm, $d^{-1} = 600$ mm^{-1}, $\lambda = 857.7$ nm, $w_{\mathrm{in}} = 1.05$ mm, $\theta_{\mathrm{in}} = 33°$, and $\theta_d = 1.7°$. From these we calculate $w_o = 13.1$ μm, $\alpha = 1.4 \times 10^{-15}$ cm/Hz, and $\beta = 9.16 \times 10^3$ cm^{-2}. The angles given are for the signal beam. The input angle for the reference was adjusted to give nearly equal (but opposite) spatial dispersion.

Fig. 8 shows data used to determine the time-to-space mapping constant of our setup. Here, both reference and signal pulses were unshaped pulses directly from the Ti:sapphire laser. A series of measurements were taken with a stepper motor stage used to vary the delay of the signal pulse with respect to the reference. A low pump power (~40 mW) was chosen for these measurements (as well as other measurements unless otherwise noted) to satisfy nondepleted pump conditions for the harmonic generation. Fig. 8 is a plot of the horizontal position of the output spot, as measured on the CCD camera, as a function of signal pulse delay for a delay range of approximately 10 ps. A straight line dependence with slope 0.8 mm/ps is observed, in good agreement with the value 0.770 mm/ps calculated from (20c).

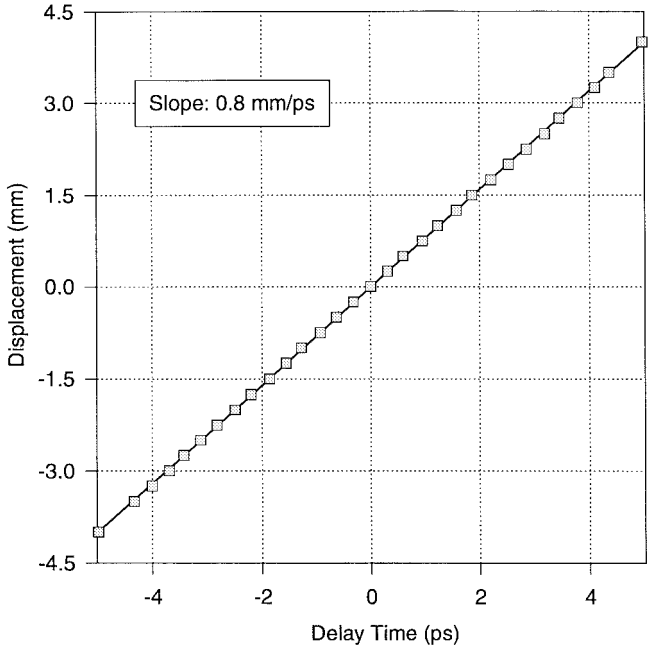

Fig. 8. Displacement of output blue beam as a function of signal pulse relative delay (with respect to reference pulse).

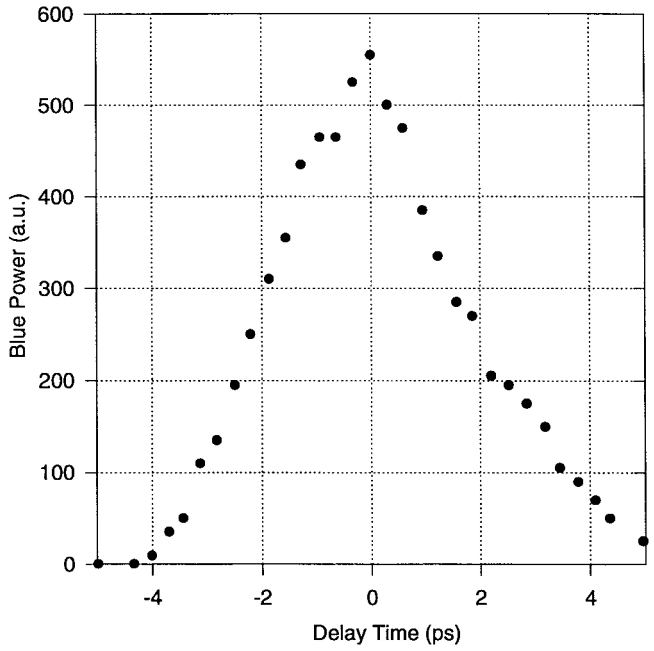

Fig. 9. Dependence of output blue power as a function of signal pulse relative delay (with respect to reference pulse).

Fig. 9 shows the power in the output spot (in arbitrary units), as a function of delay in the same measurement as for Fig. 8. The time window, within which the second-harmonic intensity remains at $\geq$50% of the intensity obtained at zero delay, is 3.9 ps. This is reasonably close the value of 3.58 ps obtained from (22). The time window data plotted in Fig. 9 does show some asymmetry not predicted in our analysis. This may arise from deviations from the assumed Gaussian beam shape.

Fig. 10 shows actual time-to-space mapping images detected by the CCD camera. In Fig. 10(a), the image shown is

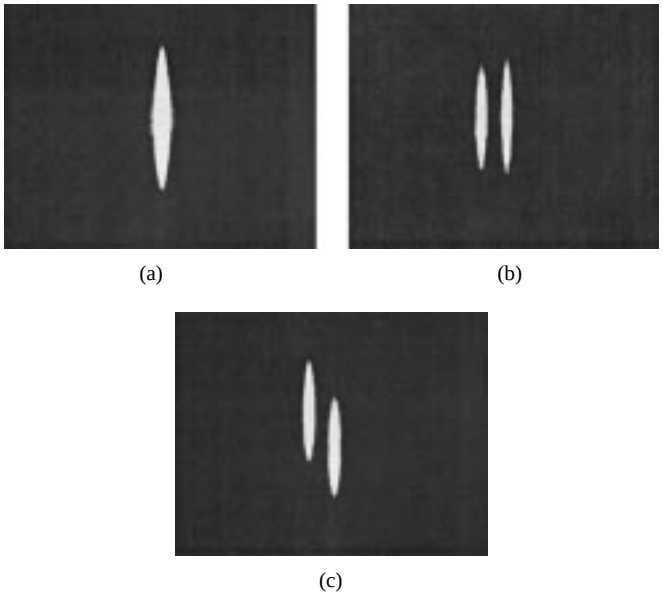

Fig. 10. Time-to-space mapping images detected by the CCD camera for an unshaped reference pulse. (a) Unshaped signal pulse. (b) Pair of signal pulses generated by inserting glass slide into the beam from the side. (c) Pair of signal pulses generated by inserting glass slide into the beam from above.

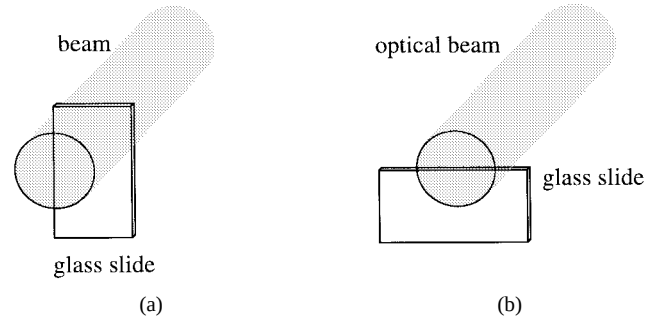

Fig. 11. Geometry for generating pulse pairs. (a) Glass slide inserted into the beam from the side. (b) Glass slide inserted into the beam from above.

for the interaction of two identical pulses with zero time delay between them. Fig. 10(b) shows the image obtained when a pair of signal pulses is generated by inserting a thin glass slide into part of the signal beam from the side [geometry shown in Fig. 11(a)]. The time-to-space process converts the signal pulse pair into a pair of two blue spots. The distance between the two spots in Fig. 10(c) was measured to be 1.3 mm, which corresponds to 1.63-ps time delay. This is in excellent agreement with the predicted value of $\tau = (n-1)s/c = 1.667$ ps, where c is the speed of light, $s = 1$ mm is the thickness of the glass slide, and $n = 1.5$ is its refractive index. Fig. 10(c) shows another image of a signal pulse doublet, where this time the doublet is created by inserting the glass slide into the signal beam from above [geometry shown in Fig. 11(b)]. Since the two signal pulses arrive at the nonlinear crystal at slightly different angles in the vertical direction, the two output spots are slightly displaced from one another in this same vertical direction. These measurements demonstrate the possibility of further mixing space and time in time–space processing, by using one spatial dimension for time-to-space conversion and the second for pure space-domain processing.

(a) (b)

Fig. 12. Time-to-space mapping images detected by the CCD camera for identical reference and signal pulse doublets. The images correspond to the correlation of the reference and signal waveforms. (a) Pulse doublets generated by inserting glass slide into beams from the side. (b) Pulse doublets generated by inserting glass slide into beams from above.

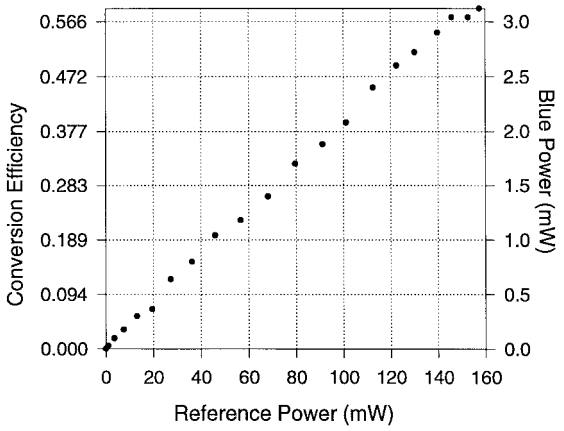

Fig. 13. Second-harmonic conversion efficiency, defined as output blue power normalized to input signal pulse power, as function of average reference pulse power. Signal pulse power is held constant at 5.3 mW. All powers are measured at the second-harmonic crystal.

However, note that the space-domain processing is limited by the phase matching acceptance angle for efficient SHG.

Fig. 12 demonstrates time-to-space conversion data for the case when both signal and reference beams are shaped. Identical pulse doublets are obtained by inserting the glass slide into the beam directly out of the laser before the beam is split into signal and reference. According to (19), the time-to-space conversion will yield an image determined by the autocorrelation of the (identical) signal and reference fields. The spatial image resulting from a pulse doublet input should then consist of a symmetric three peak structure, with the center peak more intense than the two outer peaks. The data in Fig. 12 confirm this prediction, with the glass slide inserted into the beam either from the side (a) or from the top (b). In addition to demonstrating the correlation property of time-to-space conversion, these data provide further evidence of the ability to perform time–space processing in one transverse dimension while performing pure spatial processing in the second transverse dimension.

The IR signal-to-blue conversion efficiency of this system was measured using a power meter placed at a close distance from the output facet of the crystal. The conversion efficiency of the signal beam is expected to depend linearly on the pump power. Shown in Fig. 13 is the variation of the efficiency as the average power of the reference (or pump) beam is varied for a fixed signal average power of 5.3 mW arriving at the nonlinear crystal. A linear dependence is observed. At a pump power of 160 mW (again measured at the nonlinear crystal), 3.12 mW of blue is detected corresponding to a conversion efficiency of 58%. The data presented in Fig. 13 were obtained with the signal and the reference beam aligned to propagate collinearly in the crystal. This means there is some cross-talk due to the blue light generated by the reference and the signal beams individually. Such crosstalk due to the individual beam contributions are neglected since (a) only a narrow range of input frequencies very close to ω_o are phase matched, and (b) the blue light generated from the individual beams is spread uniformly over the entire "time window" in the plane of the CCD. Nevertheless, we have also performed experiments in a noncollinear geometry that eliminates the signal from individual beams. In this case, we measure a conversion efficiency $\sim$2/3 as large as in Fig. 13.

We have analyzed the efficiency of the SHG inside the time to space converter and have found that the predicted efficiency is in reasonable agreement with the experimental results. Our efficiency analysis will be published elsewhere [4]. The key to this high-efficiency is the use of $KNbO_3$, which has a high nonlinear coefficient and which can be temperature tuned for noncritical phase matching allowing a long interaction length in the nonlinear crystal.

Finally, we analyze the temperature dependence of the SHG in our time-to-space converter. From (24), the output power $P_{\rm out}$ is proportional to

$$P_{\rm out} \sim \int e^{-(\alpha\Omega/w_o)^2} |H_{\rm PM}(\Omega)|^2 \, d\Omega. \tag{25}$$

The temperature variation of the output power is given by

$$P_{\rm out}(T) \sim \int e^{-(\alpha\Omega/w_o)^2} \left| H_{\rm PM}\left(\Omega - \frac{\partial\Omega}{\partial T}(T - T_o)\right)\right|^2 d\Omega \tag{26}$$

where $\partial\Omega/\partial T$ is the slope of the phase matching peak (in angular frequency units) vs. temperature curve, and T_o is the temperature at which the phase-matching peak coincides with $\Omega = 0$ (i.e., at second-harmonic frequency $2\omega_o$). Recall that Ω refers to the second-harmonic frequency (relative to the central SHG frequency $2\omega_o$) The phase matching spectral response function $H_{\rm PM}(\Omega)$ is given by [84]

$$|H_{\rm PM}(\Omega)|^2 = \frac{\sin^2(\Delta kL/2)}{(\Delta kL/2)^2} \tag{27a}$$

where

$$\Delta k = \left(\frac{1}{v_g}\bigg|_{\omega=2\omega_o} - \frac{1}{v_g}\bigg|_{\omega=\omega_o}\right)\Omega. \tag{27b}$$

For a group velocity mismatch of 1.2 ps/mm and a 6.2-mm crystal, we estimate the FWHM width of $|H_{\rm PM}|^2$ to be 0.073 nm, corresponding to 7.48×10^{11} rad/s. The measured variation of the phase matching peak with temperature for

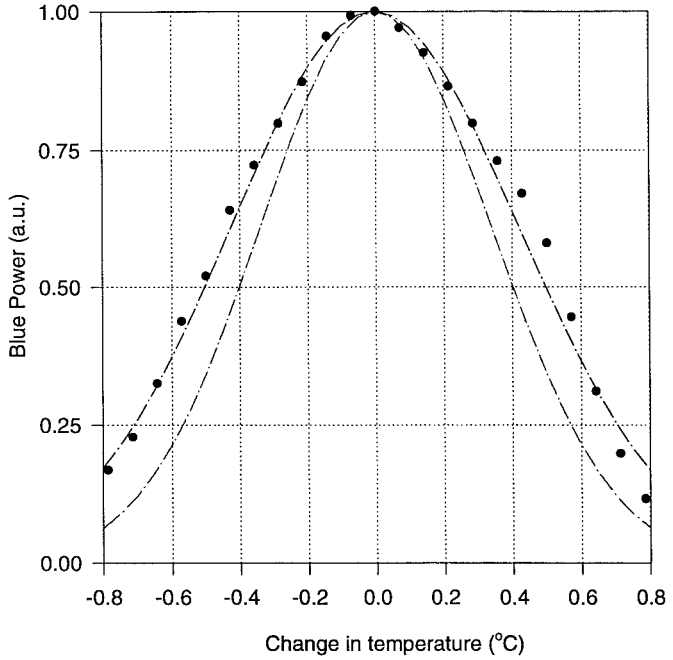

Fig. 14. Blue output power plotted as a function of crystal temperature for fixed frequency input pulses. Circles and wider dash–dot curve: data and Gaussian fit to the data. Narrower dash–dot line: theoretical temperature response curve, computed solely from the pulse-shaper spectral resolution.

our crystal is 0.188 nm/°C ($\partial\Omega/\partial T = 1.91 \times 10^{12}$ rad/s/°C). Therefore, for monochromatic input light, the temperature tuning bandwidth should be 0.39 °C. This is in reasonable agreement with the data in [57], which reported a temperature FWHM of 0.53 °C for a 5-mm $KNbO_3$ crystal (which would correspond to 0.43 °C for a 6.2-mm crystal).

The width of the $e^{-(\alpha\Omega/w_o)^2}$ term appearing in (26) is roughly 1.56×10^{12} rad/s, which is twice as wide as $|H_{\rm PM}(\Omega)|^2$. Therefore, the phase matching spectral response is narrower than the pulse-shaper spectral resolution under our experimental conditions. Thus, as a first approximation we can replace $H_{\rm PM}$ in (26) as a delta-function, with the following result for the temperature dependence of the output power:

$$P_{\rm out}(T) \sim \exp\left(-\left[\frac{\alpha}{w_o}\left(\frac{\partial\Omega}{\partial T}\right)(T - T_o)\right]^2\right). \qquad (28)$$

The temperature response is determined by the spectral resolution function of the pulse shaper. Fig. 14 shows a plot of (28), with a FWHM temperature width of 0.81 °C. Measured data (together with a Gaussian fit to the data) are also plotted, giving a 1.03 °C temperature FWHM. Both values are substantially above the 0.39 °C value calculated for conventional SHG with CW light. We can better approximate the expected temperature width if we take the finite width of $H_{\rm PM}$ into account. A rough sum-of-squares convolution yields an expected temperature width of 0.90 °C, in reasonable agreement with our data. This agreement confirms that the temperature acceptance range in the current experiments is dominated by the finite spectral resolution, which is related to the presence of a range of spectral components at any individual spatial location in the dispersed beam.

V. Summary

We have described spectral methods for shaping, processing, and time-to-space conversion of femtosecond optical pulses. Pulse-shaping techniques, which are now relatively well established, allow synthesis of nearly arbitrarily shaped ultrafast waveforms. Spectral holographic processing techniques enable storage and recall, time reversal, convolution, correlation, and matched filtering of such shaped femtosecond signals. Hybrid spectral holography systems can be used for time–space conversion of femtosecond waveforms. In order to implement more sophisticated processing of ultrafast pulse sequences, including digital logic operations, we have proposed a new generalized space–time processing concept in which input pulse sequences are first converted into the space domain, processed electronically using parallel smart pixel optoelectronic arrays, then converted back into the time domain to yield the processed output bit sequence. Such cascaded time–space systems depend critically on the ability to perform time–space conversions at the gigabit-per-second frame rates appropriate for high speed communications. For this reason we are pursuing time-to-space conversion experiments using a scheme [2], [3] based on SHG within a pulse shaper, which is consistent with these speed requirements. We have presented a detailed analysis of this time–space conversion scheme in a form that facilitates comparison with pulse-shaping theory and have described a series of experiments validating the theoretical analysis. By using a thick nonlinear crystal in a temperature tuned noncritically phase-matched geometry, we have demonstrated greater than 50% conversion efficiency in the second-harmonic crystal, which is more than two orders of magnitude higher than in previous experiments. This demonstration of high efficiency should contribute to realization of generalized time–space systems capable of performing sophisticated pulse processing operations with realistic power budgets and at frame rates suitable for high-speed communications.

Acknowledgment

The authors acknowledge D. E. Leaird for technical assistance and for help with preparation of the figures and K. T. Kornegay and L. Y. Chiou for collaboration on design of smart pixel chips for pulse processing.

References

[1] A. M. Weiner, "Femtosecond optical pulse shaping and processing," *Prog. Quantum Electron.*, vol. 19, pp. 161–238, 1995.
[2] Y. T. Mazurenko, S. E. Putilin, A. G. Spiro, A. G. Beliaev, V. E. Yashin, and S. A. Chizhov, "Ultrafast time-to-space conversion of phase by the method of spectral nonlinear optics," *Opt. Lett.*, vol. 21, pp. 1753–1755, 1996.
[3] P. C. Sun, Y. T. Mazurenko, and Y. Fainman, "Femtosecond pulse imaging: Ultrafast optical oscilloscope," *J. Opt. Soc. Amer. A*, vol. 14, p. 1159, 1997.
[4] A. M. Kan'an and A. M. Weiner, "Efficient time-to-space conversion of femtosecond optical pulses," *J. Opt. Soc. Amer. B*, vol. 15, pp. 1242–1245, 1998.
[5] A. M. Weiner, J. P. Heritage, and E. M. Kirschner, "High-resolution femtosecond pulse shaping," *J. Opt. Soc. Amer. B*, vol. 5, pp. 1563–1572, 1988.
[6] A. M. Weiner, D. E. Leaird, J. S. Patel, and J. R. Wullert, "Programmable shaping of femtosecond pulses by use of a 128-element liquid-crystal phase modulator," *IEEE J. Quantum Electron.*, vol. 28, pp. 908–920, 1992.

[7] C. Froehly, B. Colombeau, and M. Vampouille, "Shaping and analysis of picosecond light pulses," in *Progress in Optics*, E. Wolf, Ed., Amsterdam, The Netherlands: North-Holland, 1983, vol. 20, pp. 65–153.

[8] J. P. Heritage, A. M. Weiner, and R. N. Thurston, "Picosecond pulse shaping by spectral phase and amplitude manipulation," *Opt. Lett.*, vol. 10, p. 609, 1985.

[9] A. M. Weiner, J. P. Heritage, and R. N. Thurston, "Synthesis of phase coherent, picosecond optical square pulses," *Opt. Lett.*, vol. 11, p. 153, 1986.

[10] A. M. Weiner and J. P. Heritage, "Picosecond and femtosecond Fourier pulse shape synthesis," *Rev. Phys. Appl.*, vol. 22, p. 1619, 1987.

[11] A. M. Weiner, J. P. Heritage, and J. A. Salehi, "Encoding and decoding of femtosecond pulses," *Opt. Lett.*, vol. 13, pp. 300–302, 1988.

[12] D. H. Reitze, A. M. Weiner, and D. E. Leaird, "Shaping of wide bandwidth 20 fsec optical pulses," *Appl. Phys. Lett.*, vol. 61, pp. 1260–1262, 1992.

[13] A. Efimov, C. Schaffer, and D. H. Reitze, "Programmable shaping of ultrabroad-bandwidth pulses from a Ti:sapphire laser," *J. Opt. Soc. Amer. B*, vol. 12, pp. 1968–1980, 1995.

[14] O. E. Martinez, "3000 times grating compressor with positive group velocity dispersion: Application to fiber compensation in 1.3–1.6 μm region," *IEEE J. Quantum Electron.*, vol. 23, p. 59, 1987.

[15] A. M. Weiner, Y. Silberberg, H. Fouckhardt, D. E. Leaird, M. A. Saifi, M. J. Andrejco, and P. W. Smith, "Use of femtosecond square pulses to avoid pulse breakup in all-optical switching," *IEEE J. Quantum Electron.*, vol. 25 p. 2648, 1989.

[16] A. M. Weiner and D. E. Leaird, "Generation of terahertz-rate trains of femtosecond pulses by phase-only filtering," *Opt. Lett.*, vol. 15, pp. 51–53, 1990.

[17] A. M. Weiner, S. Oudin, D. E. Leaird, and D. H. Reitze, "Shaping of femtosecond pulses using phase-only filters designed by simulated annealing," *J. Opt. Soc. Amer. A*, vol. 10, pp. 1112–1120, 1993.

[18] H. Dammann and K. Gortler, "High-efficiency in-line multiple imaging by means of multiple phase holograms," *Opt. Commun.*, vol. 3, pp. 312–315, 1971.

[19] U. Killat, G. Rabe, and W. Rave, "Binary phase gratings for star couplers with high splitting ratios," *Fiber Integ. Opt.*, vol. 4, 1982.

[20] A. M. Weiner, D. E. Leaird, J. S. Patel, and J. R. Wullert, "Programmable femtosecond pulse shaping by using a multielement liquid crystal phase modulator," *Opt. Lett.*, vol. 15, pp. 326–328, 1990.

[21] M. M. Wefers and K. A. Nelson, "Generation of high-fidelity programmable ultrafast optical waveforms," *Opt. Lett.*, vol. 20, pp. 1047–1049, 1995.

[22] M. Ratsep, M. Tian, I. Lorgere, F. Grelet, and J.-L. L. Gouet, "Fast random access to frequency-selective optical memories," *Opt. Lett.*, vol. 21, pp. 83–85, 1996.

[23] C. W. Hillegas, J. X. Tull, D. Goswami, D. Strickland, and W. S. Warren, "Femtosecond laser pulse shaping by use of microsecond radio-frequency pulses," *Opt. Lett.*, vol. 19, pp. 737–739, 1994.

[24] E. A. D. Souza, M. C. Nuss, W. H. Knox, and D. A. B. Miller, "Wavelength-division multiplexing with femtosecond pulses," *Opt. Lett.*, vol. 20, pp. 1166–1168, 1995.

[25] K. Ema, N. Kagi, and F. Shimizu, "Optical compression using a monochromator and a concave mirror," *Opt. Commun.*, vol. 71, p. 103, 1989.

[26] K. F. Kwong, D. Yankelevich, K. C. Chu, J. P. Heritage, and A. Dienes, "400-Hz mechanical scanning optical delay line," *Opt. Lett.*, vol. 18, pp. 558–560, 1993.

[27] J. P. Heritage, E. W. Chase, R. N. Thurston, and M. Stern, "A simple femtosecond optical third-order disperser," in *Conf. Lasers and Electro-Optics*, Opt. Soc. Amer., Baltimore, MD, 1991, pp. 74–75.

[28] K. Ema and F. Shimizu, "Optical pulse shaping using a Fourier-transformed hologram," *Jpn. J. Appl. Phys.*, vol. 29, p. 1458, 1990.

[29] A. M. Weiner, D. E. Leaird, D. H. Reitze, and E. G. Paek, "Femtosecond spectral holography," *IEEE J. Quantum Electron.*, vol. 28, pp. 2251–2261, 1992.

[30] M. C. Nuss and R. L. Morrison, "Time-domain images," *Opt. Lett.*, vol. 20, pp. 740–742, 1995.

[31] Y. Ding, R. M. Brubaker, D. D. Nolte, M. R. Melloch, and A. M. Weiner, "Femtosecond pulse shaping by dynamic holograms in photorefractive multiple quantum wells," *Opt. Lett.*, vol. 22, pp. 718–720, 1997.

[32] Y. Ding, D. D. Nolte, M. R. Melloch, and A. M. Weiner, "Real-time edge enhancement of femtosecond time-domain images," *Opt. Lett.*, vol. 17, pp. 1101–1103, 1997.

[33] A. M. Weiner, J. P. Heritage, R. J. Hawkins, R. N. Thurston, E. M. Kirschner, D. E. Leaird, and W. J. Tomlinson, "Experimental observation of the fundamental dark soliton in optical fibers," *Phys. Rev. Lett*, vol. 61, p. 2445 1988.

[34] A. M. Weiner, R. N. Thurston, W. J. Tomlinson, J. P. Heritage, D. E. Leaird, E. M. Kirschner, and R. J. Hawkins, "Temporal and spectral self-shifts of dark optical solitons," *Opt. Lett.*, vol. 14, p. 868, 1989.

[35] A. M. Weiner, D. E. Leaird, G. P. Wiederrecht, and K. A. Nelson, "Femtosecond pulse sequences used for optical control of molecular motion," *Science*, vol. 247, p. 1317, 1990.

[36] I. Brener, P. C. M. Planken, M. C. Nuss, M. S. C. Luo, S. L. Chuang, L. Pfeiffer, D. E. Leaird, and A. M. Weiner, "Coherent control of THz emission and carrier populations in semiconductor heterostructures," *J. Opt. Soc. Amer. B*, vol. 11, pp. 2457–2569, 1994.

[37] Y. Liu, S.-G. Park, and A. M. Weiner, "Enhancement of narrowband terahertz radiation from photoconducting antennas by optical pulse shaping," *Opt. Lett.*, vol. 21, pp. 1762–1764, 1996.

[38] Y. Liu, S.-G. Park, and A. M. Weiner, "Terahertz waveform synthesis via optical pulse shaping," *IEEE J. Select. Topics Quantum Electron.*, vol. 2, pp. 709–719, 1996.

[39] J. S. Patel and Y. Silberberg, "Liquid crystal and grating based multiple-wavelength cross-connect switch," *IEEE Photon. Technol. Lett.*, vol. 7, pp. 514–516, 1995.

[40] J. E. Ford, J. A. Walker, M. C. Nuss, and D. A. B. Miller, "32 channel WDM graphic equalizer," presented at the 1996 Summer Top. Meet. Broadband Optical Networks, Keystone, CO, 1996.

[41] J. E. Ford, A. V. Krishnamoorthy, S. Tsuda, W. H. Knox, M. C. Nuss, and D. A. B. Miller, "WDM/SDM fiber network design for the AMOEBA optoelectronic switch," presented at the 1996 Summer Top. Meet. Smart Pixels, Keystone, CO, 1996.

[42] A. M. Weiner, J. A. Salehi, J. P. Heritage, and M. Stern, "Encoding and decoding of femtosecond pulses for code-division multiple-access," in *OSA Proceedings on Photonic Switching*, J. E. Midwinter and H. S. Hintons, Eds. Washington, DC: Opt. Soc. Amer., 1989, vol. 3, pp. 263–269.

[43] J. A. Salehi, A. M. Weiner, and J. P. Heritage, "Coherent ultrashort light pulse code-division multiple access communication systems," *J. Lightwave Technol.*, vol. 8, p. 478, 1990.

[44] A. M. Weiner and J. A. Salehi, "Optical code-division multiple-access," *in Photonics in Switching*, J. Midwinter, Ed. San Diego, CA: Academic, 1993, vol. II, pp. 73–118.

[45] D. Zaccarin and M. Kavehrad, "An optical CDMA system based on spectral encoding of LED," *IEEE Photon. Technol. Lett.*, vol. 5, pp. 479–482, 1993.

[46] L. Nguyen, T. Dennis, B. Aazhang, and J. F. Young, "Experimental demonstration of bipolar codes for optical spectral amplitude CDMA communication," *J. Lightwave Technol.*, vol. 15, pp. 1647–1653, 1997.

[47] H. P. Sardesai and A. M. Weiner, "Nonlinear fiber-optic receiver for ultrashort pulse code-division multiple-access communications," *Electron. Lett.*, vol. 33, pp. 610–611, 1997.

[48] C.-C. Chang, H. P. Sardesai, and A. M. Weiner, "Code-division multiple-access encoding and decoding of femtosecond optical pulses over a 2.5-km fiber link," *IEEE Photon. Technol. Lett.*, vol. 10. pp. 171–173, 1998.

[49] C.-C. Chang, H. P. Sardesai, and A. M. Weiner, "Dispersion-free fiber transmission for femtosecond pulses using a dispersion-compensating fiber and a programmable pulse shaper," *Opt. Lett.*, vol. 23, pp. 283–285, 1998.

[50] H. Shi, J. Finlay, G. Alphonse, J. Connolly, and P. J. Delfyett, "Multiwavelength 10 GHz picosecond pulse generation from a single-stripe semiconductor diode laser," *J. Lightwave Technol.*, vol. 9, pp. 1439–1441, 1997.

[51] V. Binjrajka, C.-C. Chang, A. W. R. Emanuel, D. E. Leaird, and A. M. Weiner, "Pulse shaping of incoherent light by use of a liquid crystal modulator array," *Opt. Lett.*, vol. 21, pp. 1756–1758, 1996.

[52] R. A. Griffin, D. D. Sampson, and D. A. Jackson, "Coherence coding for code-division multiple-access networks," *J. Lightwave Technol.*, vol. 13, pp. 1826–1837, 1995.

[53] H. Soañajalg, A. Débarre, J.-L. L. Gouët, I. Lorgeré, and P. Tchénio, "Phase-encoding technique in time-domain holography: Theoretical estimation," *J. Opt. Soc. Amer. B*, vol. 12, pp. 1448–1459, 1995.

[54] K. M. Mahoney and A. M. Weiner, "Modified femtosecond pulse shaper using microlens arrays," *Opt. Lett.*, vol. 21, pp. 812–814, 1996.

[55] K. M. Mahoney and A. M. Weiner, "A femtosecond pulse shaping apparatus containing microlens arrays for use with pixellated spatial light modulators," *IEEE J. Quantum Electron.*, vol. 32, pp. 2017–2077, 1996.

[56] R. N. Thurston, J. P. Heritage, A. M. Weiner, and W. J. Tomlinson, "Analysis of picosecond pulse shape synthesis by spectral masking in a grating pulse compressor," *IEEE J. Quantum Electron.*, vol. 22, pp. 682–696, 1986.

[57] M. B. Danailov and I. P. Christov, "Time-space shaping of light pulses by Fourier optical processing," *J. Modern Opt.*, vol. 36, pp. 725–731, 1989.
[58] M. M. Wefers and K. A. Nelson, "Space-time profiles of shaped ultrafast optical waveforms," *IEEE J. Quantum Electron.*, vol. 32, pp. 161–172, 1996.
[59] J. Paye and A. Migus, "Space-time Wigner functions and their application to the analysis of a pulse shaper," *J. Opt. Soc. Amer. B*, vol. 12, pp. 1480–1491, 1995.
[60] I. Lorgere, M. Ratsep, J.-L. L. Gouet, F. Grelet, M. Tian, A. Debarre, and P. Tchenio, "Storage of spectrally shaped hologram in a frequency selective material," *J. Phys. B: At. Mol. Opt. Phys.*, vol. 28, pp. L565–L570, 1995.
[61] Y. T. Mazurenko, "Holography of wave packets," *Appl. Phys. B*, vol. 50, pp. 101–114, 1990.
[62] A. M. Weiner, D. E. Leaird, D. H. Reitze, and E. G. Paek, "Spectral holography of shaped femtosecond pulses," *Opt. Lett.*, vol. 17, pp. 224–226, 1992.
[63] A. M. Weiner and D. E. Leaird, "Femtosecond signal processing by second order spectral holography," *Opt. Lett.*, vol. 19, pp. 123–125, 1994.
[64] Y. T. Mazurenko, "Time-domain Fourier transform holography and possible applications in signal processing," *Opt. Eng.*, vol. 31, pp. 739–749, 1992.
[65] K. Ema, M. Kuwata-Gonokami, and F. Shimizu, "All-optical sub-Tbits/s serial-to-parallel conversion using excitonic giant nonlinearity," *Appl. Phys. Lett.*, vol. 59, pp. 2799–2801, 1991.
[66] K. Ema, "Real-time ultrashort pulse shaping and pulse-shape measurement using a dynamic grating," *Jpn. J. Appl. Phys.*, vol. 30, pp. L2046–L2049, 1991.
[67] M. C. Nuss, M. Li, T. H. Chiu, A. M. Weiner, and A. Partovi, "Time-to-space mapping of femtosecond pulses," *Opt. Lett.*, vol. 19, pp. 664–666, 1994.
[68] P. C. Sun, Y. T. Mazurenko, W. S. C. Chang, P. K. L. Yu, and Y. Fainman, "All-optical parallel-to-serial conversion by holographic spatial-to-temporal frequency encoding," *Opt. Lett.*, vol. 20, pp. 1728–1730, 1995.
[69] A. Partovi, A. M. Glass, D. H. Olson, G. J. Zydzik, H. M. O'Bryan, T. H. Chiu, and W. H. Knox, "Cr-doped GaAs/AlGaAs semi-insulating multiple quantum well photorefractive devices," *Appl. Phys. Lett.*, vol. 62, pp. 464–466, 1993.
[70] D. Nolte and M. Melloch, "Bandgap and defect engineering for semiconductor holographic materials: Photorefractive quantum wells and thin films," *MRS Bull.*, vol. 19, pp. 44–49, 1994.
[71] S. R. Forrest and H. S. Hinton, Eds., *IEEE J. Quantum Electron.* (special issue on smart pixels), vol. 29, pp. 598–813, 1993.
[72] A. L. Lentine and D. A. B. Miller, "Evolution of the SEED technology: Bistable logic gates to optoelectronic smart pixels," *IEEE J. Quantum Electron.*, vol. 29, pp. 655–669, 1993.
[73] K. W. Goossen, J. A. Walker, L. A. D'Asaro, S. P. Hui, B. Tseng, R. Leigenbuth, D. Kossives, D. D. Bacon, D. Dahringer, L. M. F. Chrirovsky, A. L. Lentine, and D. A. B. Miller, "GaAs MQW modulators integrated with silicon CMOS," *IEEE Photon. Technol. Lett.*, vol. 7, pp. 360–362, 1995.
[74] M. Whitehead and G. Parry, "High-contrast reflection modulation at normal incidence in asymmetric multiple quantum well Fabry–Perot structure," *Electron. Lett.*, vol. 25, pp. 566–568, 1989.
[75] R. H. Yan, R. J. Simes, and L. A. Coldren, "Electroabsorptive Fabry-Perot reflection modulators with asymmetric mirrors," *IEEE Photon. Technol. Lett.*, vol. 1, pp. 273–275, 1989.
[76] G. B. Thompson, G. Robinson, J. W. Scott, C. J. Mahon, F. H. Peters, B. J. Thibeault, and L. A. Coldren, "1×18 array of low voltage, asymmetric Fabry–Perot modulators for gigabit data transmission applications," presented at the IEEE/LEOS Summer Top. Meet. Smart Pixels, Lake Tahoe, NV, 1994.
[77] S. J. B. Yoo, R. Bhat, C. Caneau, J. Gamelin, M. A. Koza, and T. P. Lee, "High-speed 1.5 micron asymmetric Fabry–Perot modulators," presented at the Optical Fiber Communications Conf., San Diego, CA, 1995.
[78] J. C. Baumert and P. Günter, "Noncritically phase-matched sum-frequency generation and image up-conversion in $KNbO_3$ crystals," *Appl. Phys. Lett.*, vol. 50, pp. 554–556, 1987.
[79] U. Ellenberger, R. Weber, J. E. Balmer, B. Zysset, D. Ellgehausen, and G. Mizell, "Pulse optical damage threshold of potassium niobate," *Appl. Opt.*, vol. 31, pp. 7563–7569, 1992.
[80] B. Zysset, I. Biaggio, and P. Günter, "Refractive indices of orthorhombic $KNbO_3$. I. Dispersion and temperature dependence," *J. Opt. Soc. Amer. B*, vol. 9, pp. 380–386, 1992.
[81] I. Biaggio, P. Kerkoc, L. S. Wu, P. Günter, and B. Zysset, "Refractive indices of orthorhombic $KNbO_3$. II. Phase-matching configurations for nonlinear optical interactions," *J. Opt. Soc. Amer. B*, vol. 9, pp. 507–517, 1992.
[82] O. E. Martinez, "Grating and prism compressors in the case of finite beam size," *Opt. Soc. Amer. B*, vol. 3, pp. 929–934, 1986.
[83] J. Comly and E. Garmire, "Second harmonic generation from short pulses," *Appl. Phys. Lett*, vol. 12, pp. 7–9, 1968.
[84] W. H. Glenn, "Second-harmonic generation by picosecond optical pulses," *IEEE J. Quantum Electron.*, vol. QE-5, pp. 281–290, 1969.
[85] S. A. Akhmanov, A. P. Sukhorukov, and A. S. Chirkin, "Nonstationary phenomena and space-time analogy in nonlinear optics," *Soviet Phys. JETP*, vol. 28, pp. 748–757, 1969.
[86] J. W. Goodman, *Introduction to Fourier Optics*. New York: McGraw-Hill, 1968.
[87] K. Kato, "High efficiency second harmonic generation at 4250–4680 Å in $KNbO_3$," *IEEE J. Quantum Electron.*, vol. 15, pp. 410–411, 1979.

A. M. Weiner (S'84–M'84–SM'91–F'95) received the Sc.D. degree in electrical engineering from the Massachusetts Institute of Technology (M.I.T.), Cambridge, in 1984, and was a Fannie and John Hertz Foundation Graduate Fellow at M.I.T. from 1979 to 1984. His doctoral thesis dealt with femtosecond pulse compression (including generation of the shortest optical pulses reported up to that time) and measurement of femtosecond dephasing in condensed matter.

In 1984, he joined Bellcore, where he conducted research on ultrafast optics, including shaping of ultrashort pulses and nonlinear optics and switching in fibers. In 1989, he became Manager of the Ultrafast Optics and Optical Signal Processing Research District. He assumed his current position as Professor of electrical and computer engineering at Purdue University, West Lafayette, IN, in 1992. Since 1996, he has also served as Director of Graduate Admissions, School of Electrical and Computer Engineering. He has spoken at approximately 170 conference and university talks and has authored or co-authored approximately 100 technical articles, including three book chapters. He holds five U.S. patents. His current research interests center on holography of ultrashort pulses, high-speed optical communications, applications of pulse shaping to femtosecond spectroscopy and nonlinear optics, and optical imaging in scattering media. He is a Topical Editor of *Optics Letters.* He has served as vice-chairman of the Gordon Conference on Nonlinear Optics and Lasers, chair of the Ultrafast Phenomena Technical Group of the Optical Society of America (OSA), and chair of the OSA Lomb Medal Committee. He was program co-chair (1996) and general co-chair (1998) for the Conference on Laser and Electro-Optics.

Prof. Weiner is a Fellow of the OSA and a member of the IEEE Lasers and Electro-Optics Society (LEOS) Board of Governors. He has served as Associate Editor of the IEEE JOURNAL OF QUANTUM ELECTRONICS AND OF PHOTONICS TECHNOLOGY LETTERS. He has served on the IEEE Education Medal Committee and of the IEEE Quantum Electronics Award Committee, and member of numerous conference committees. From 1988 to 1989, he served as IEEE LEOS traveling lecturer. In 1984, he was the recipient of the 1984 Hertz Foundation Doctoral Thesis Prize. In 1990, he was awarded the Adolph Lomb Medal of the OSA for noteworthy contributions to optics made before reaching the age of 30, and was also recipient of the 1997 ASEE Curtis W. McGraw Research Award and the 1997 Prize of the International Commission on Optics.

Ayman M. Kan'an, photograph and biography not available at the time of publication.